

Spectroscopic study of excess electrons in liquid helium

A. Ya. Parshin and S. V. Pereverzev

P. L. Kapitza Institute of Physical Problems, Academy of Sciences of the USSR

(Submitted 16 August 1991)

Zh. Eksp. Teor. Fiz. **101**, 126–142 (January 1992)

The optical absorption spectra of electrons self-trapped in microscopic bubbles in liquid helium have been measured over the wavelength interval 5–8.5 μm . The characteristics of the $1s-1p$ absorption line have been studied as a function of the pressure (over the range 2–40 atm) and the temperature (2–4 K). The observed changes in the position of the center of the line with the temperature and the pressure can be described in a simple model of a bubble, by introducing the effective surface tension of the bubble boundary as an adjustable parameter. The absorption line turns out to be much wider than predicted by the theory. Data on the position of the line agree well with photomobility experiments.

1. INTRODUCTION

Charged particles in liquid helium form rather complicated complexes with surrounding atoms. Research on these complexes has emerged as a separate trend in helium physics. One of the most interesting entities of this sort is a bubble formed in liquid helium by an excess electron. The reason for the formation of such a bubble is the strong repulsion between an electron and a helium atom at short range.

In a simple model, the energy of the electron in a bubble can be found as the energy of the ground state of a particle of mass m in a spherical potential well of radius a and depth U_0 (U_0 is the work involved in the penetration of an electron into liquid helium in a process not accompanied by the formation of a bubble). The equilibrium bubble radius a is determined by the balance between the pressure exerted on the wall by the electron and the sum of the Laplace and hydrostatic pressures. A model of this sort was first proposed by Ferrel¹ in an effort to explain the anomalously long lifetime of positronium in liquid helium.

The bubble model agrees well with extensive data on the mobility of ions under various conditions, with measurements of effective masses, and with experiments on the trapping of electrons by vortex threads (see, for example, the review by Shikin²). The bubble radius estimated from the results of various experiments (10–20 Å) is large in comparison with the interatomic distance, while the effective thickness of the bubble wall is at the atomic scale according to the theory of Refs. 3–5. We thus have grounds for treating a bubble as a potential well with vertical walls.

In a spherical potential well with a square potential, the bound states arise in the following order with increasing well depth: $1s$, $1p$, $1d$, $2s$, $1f$, $2p$, ... (Ref. 6). In a real situation, the number of such states will of course be bounded. According to Ref. 7, for example, the $2p$ states appears only at pressures below 20 atm. These comments apply to wells with rigid walls. If a possible deformation of the bubble is taken into account, the effective potential well for each electronic state will have its own equilibrium shape, and the order of levels given above may in general change. An important point for the discussion below is that the ground state is spherically symmetric. Although this assumption has not previously been questioned, to the best of our knowledge the equilibrium shape of a bubble for an arbitrary electronic state has not

been finally resolved.

Estimates of the characteristics of electron transitions induced by light in a bubble are usually based on the Franck-Condon principle; i.e., it is assumed that the transition is not accompanied by any change in the configuration of the surrounding helium atoms. Calculations of this sort can be found in papers by various investigators.^{3,7–10} The oscillator strengths for $1s-1p$ and $1s-2p$ transitions are 0.97 and 0.025, respectively, and depend weakly on the pressure.^{7,11} The smearing of the potential at the bubble boundaries has only a slight effect on the energies of the deep levels, and this model should provide a reliable estimate of the position of the $1s \rightarrow 1p$ absorption line. There is accordingly much interest in the acquisition of direct spectroscopic data.

In actual experiments, it is rather difficult to raise the density of self-trapped electrons of this sort in liquid helium to a level sufficient for direct measurement of optical absorption. On the other hand, it has been found possible to detect an effect of light on the mobility of these electrons. At sufficiently low temperatures the ions in a strong electric field create vortex rings and move along with these rings. Under these conditions, an electron transition may result in the release of an electron bubble from the core of a vortex ring. The ion will have a high mobility until a new vortex forms. This effect was first observed by Northby and Sanders.¹² The increase in the mobility of negative ions for exciting light at a wavelength near 2 μm was subsequently interpreted by Miyakawa and Dexter⁸ as corresponding to the $1s \rightarrow 2p$ transition, and the mobility peak near 1 μm was attributed to transitions to the continuum. The $1s \rightarrow 2p$ transition was recently observed by a similar method by Grimes and Adams.¹³

With increasing temperature, the probability for the liberation of a bubble from the core of a vortex ring as the result of collisions with thermal phonons increases. The increase in the electron mobility due to the light becomes unobservable even at temperatures above 1.3 K. Furthermore, at pressures above 17 atm the negative ions cease to create vortex rings. At low temperatures, the creation of rotons becomes the primary mechanism for the slowing of these ions as they move in the electric field. The photomobility effect fades away.¹³

In the present experiments we have directly measured the absorption of light during $1s \rightarrow 1p$ electron transitions. These experiments were reported briefly in Ref. 14.

2. EXPERIMENTAL APPARATUS

Observing a low level of optical absorption requires a light source with a high stability and a high spectral brightness. We used semiconductor lasers (see the review by Zsavitvskii¹⁵), which have no peers in terms of these characteristics in the spectral region of interest here, 5–10 μm . For our particular case, the spectral interval over which a laser of this type can be tuned is small in comparison with the expected width of the absorption line. However, one could make use of the strong pressure dependence of the equilibrium bubble radius and thus of the frequency of the electron transition. In the experiments we slowly varied the helium pressure and monitored the resonant absorption of light when the frequency of the electron transition in the bubble became equal to the fixed laser output frequency. The concentration of electrons was modulated by an electric field; the absorption signal was measured at the modulation frequency. The spectral sensitivity was achieved through the use of a set of semiconductor lasers with known frequencies. These lasers operated at liquid-helium temperature and were installed in the apparatus in succession.

The laser beam entered the test chamber with the helium through a short length (60 mm) of (KRS)-13 optical fiber in (AgCl) cladding (Fig. 1). Inside the test chamber, the fiber passed through a gap 1 mm wide between two plane stainless steel electrodes. A molybdenum plate coated with a layer of titanium tritide (a standard ionizer, with a saturation current $j_{\text{sat}} = 1.4 \cdot 10^{-8}$ A/cm²) was mounted on the surface of one of these stainless steel electrodes. As the light propagated between the electrodes, it struck a photoresistance (SiB). The light was absorbed over a distance of 40 mm, which was set by the geometry of the β source. A plane-parallel NaCl plate had to be placed between the electrodes and the photoresistance to prevent leakage of the ion current to the photoresistance.

The lasers were mounted in a small vacuum chamber in such a way that the laser crystal was in front of the entrance end of the fiber. The typical cross section of this crystal, 0.3·0.3 mm², is significantly smaller than the fiber diameter (0.7 mm without the cladding). We managed to do without an adjustment of the cold apparatus.

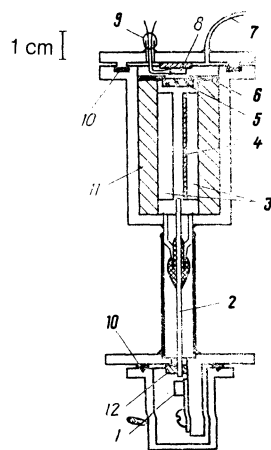


FIG. 1. Test cell. 1—Laser crystal; 2—optical fiber; 3—electrodes; 4—ionizer; 5—NaCl plate; 6—copper shield; 7—filling capillary; 8—photoresistance; 9—current leads; 10—glass-fabric-based-laminate housing; 11—In packing; 12—holder for the entrance end of the fiber.

In the experiments, the entire apparatus in the assembly was immersed in liquid helium. The temperature was monitored on the basis of the helium vapor pressure in the cryostat.

This design eliminated difficulties in coupling light at a wavelength near the thermal-emission peak at room temperature into the cryostat. In addition, low-frequency vibrations of the cryostat would certainly have affected the stability of the light flux during the coupling of light in from the exterior. The natural mechanical vibrations of the apparatus, in contrast, are of high frequency and are not seen in the frequency range of interest here, 20–30 Hz.

To maintain the necessary pressure of the prepurified helium in the test chamber, we used a gasifier like that described in Ref. 16. The pressure in the system was measured by a mechanical gauge and also by an absolute-pressure converter with a semiconductor strain gauge. The signal from this converter was used in a feedback system to control the gasifier and to stabilize the pressure or to vary it linearly in time.

3. STRUCTURE OF THE LAYER OF IONIZED HELIUM NEAR THE β SOURCE; ION DENSITY IN THE DRIFT VOLUME

The tritium source causes ionization in a thin helium layer with a thickness Δ (which is on the order of 10 μm ; Ref. 17). The ions can be extracted from this layer into the volume between the electrodes by means of an electric field. Figure 2 shows the ion current as a function of the voltage applied to the electrodes. Curves of this sort have been seen previously.^{17,18} The + in this figure corresponds to the pressure in the electron drift volume. At the beginning of the positive branch there is a short quadratic region, which corresponds to the classical Thomson case, in which the space

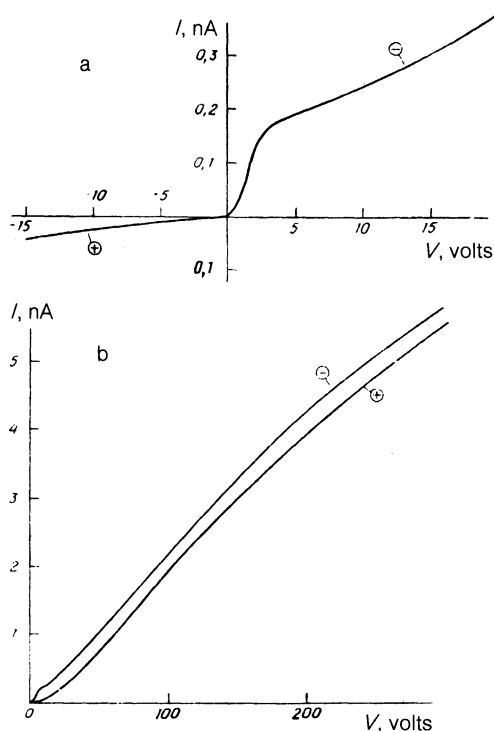


FIG. 2. Static current-voltage characteristics measured at a temperature of 4.2 K and a pressure of 2 atm. The area of the electrodes is 1.6 cm², and the distance between them is 0.5 mm.

charge between the electrodes completely screens the external electric field from the ion source ($E_{\text{src}} = 0$). In this regime we have

$$j = 32\pi\mu V^2/9d^3, \quad (1)$$

where j is the current density, V is the applied voltage, d is the distance between electrodes, and μ is the ion mobility. The average ion density in the drift volume under these conditions is determined by the applied voltage and is independent of the ion mobility:

$$\bar{n} = \frac{1}{d} \int_0^d n(x) dx = \frac{3V}{8\pi ed^2}. \quad (2)$$

The quadratic region ends when the ion current reaches a level on the order of the current of the primary β particles. In other words, at $E_{\text{src}} = 0$ essentially all the secondary ions recombine inside the ionized layer. A further increase in the current requires a separation of the ions in the ionized layer by the electric field, and the condition $E_{\text{src}} = 0$ should be violated.

At currents well above the current of primary β particles, the electric field required for charge separation in the ionized layer is much stronger than the space-charge field. In this case the ions drift in an essentially uniform field $\bar{E} = V/d$ in the volume between the electrodes, and the ion density can be estimated from $\bar{n} = jd/e\mu V$. At a current $I = 10^{-9}$ A, which amounts to $0.04I_{\text{sat}}$ and which is about seven times the current of primary β particles, the field \bar{E} is 1000 V/cm. In this case \bar{n} , is on the order of $2 \cdot 10^8$ ions/cm³, and the space-charge field does not exceed $2\pi e\bar{n}d \approx 10$ V/cm.

By increasing the average field in the gap between the electrodes, we separate a progressively large number of ions in the ionized layer. However, the ion drift time between the electrodes falls off at the same time, and the average density in the drift volume remains roughly constant.

It is a simple matter to estimate the maximum ion density in the ionized layer: It is the density in the case of an ionization which is uniform over volume. At equilibrium, the decrease in the number of ions due to recombination is offset by the creation of new pairs, and we can write

$$\frac{dn}{dt} = -\Delta\alpha n^2 + \frac{j_{\text{sat}}}{e} = 0. \quad (3)$$

Here α is the recombination coefficient, which has a value $\alpha \approx 10^{-7}$ ions/cm³ at $T = 4.2$ K (Ref. 19). We thus find $n \approx 3 \cdot 10^{10}$ ions/cm³. We can estimate the electric field characterizing the interaction of the ions in the ionized layer:

$$E_{\text{exp}} \approx en^{2/3} \approx 1.5 \text{ V/cm}.$$

Another important quantity is the maximum electric field which can be screened in the ionized layer as a result of its polarization. We can write this field as $E_{\text{exp}} \approx 4\pi en\Delta \approx 50$ V/cm. These simple estimates show that the application of an external electric field on the order of 1000 V/cm to a uniformly ionized layer should lead to an essentially complete separation of the ions in this layer. In other words, the current should be close to the saturation current. The experimental fact that the ion current in such a field amounts to only 1/25 of the saturation current demonstrates that the ion

distribution in the ionized layer is highly nonuniform. We might suggest that compact clusters of ions and isolated electron-(positive ion) pairs, with a short distance between charges, form at the tracks of the primary β particles. Such pairs should appear when the energy of a secondary electron is insufficient to cause yet another ionization event. The suggestion that low-energy secondary electrons in condensed helium have a short range with respect to trapping (i.e., with respect to the formation of a bubble) has been discussed previously.²⁰

It is the small value of this distance between the charges in the electron-ion pairs (in the ion clusters) formed at the tracks of the fast particles which prevents the attainment of high ion densities in condensed helium, regardless of the ionization method.

A point of importance for our purposes is that the average electron density in the drift volume can be raised substantially if the ionized layer is rendered more nearly uniform by separating and mixing the electron-ion pairs, by means of a strong alternating electric field of fairly high frequency (on the order of 10^5 – 10^6 Hz). In this case, a weak static drift field is sufficient to achieve ion currents of significance (in comparison with the current of primary β particles.). The amplitude of the displacement of the ions caused by this alternating field must of course be small in comparison with the distance between electrodes. Figure 3 shows the ion current as a function of the drift voltage for various amplitudes of the high-frequency voltage applied to the electrodes. The quadratic region, which is now seen on both

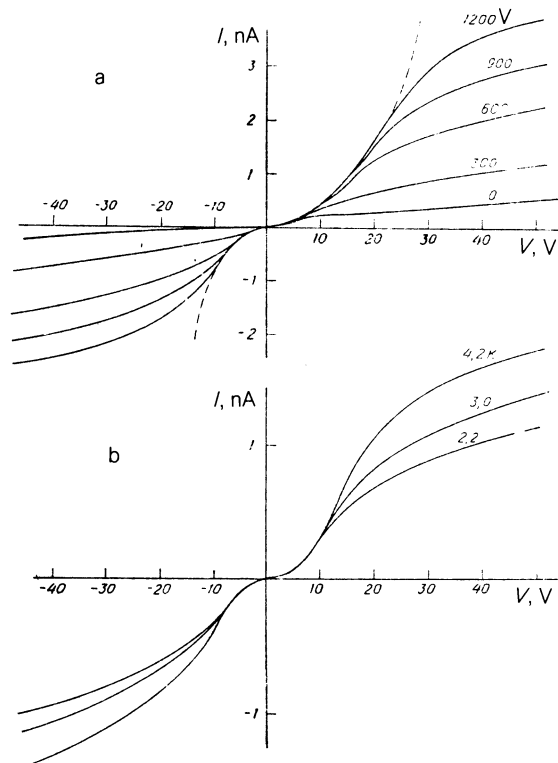


FIG. 3. a—Drift current-voltage characteristics at various amplitudes of the high-frequency voltage between the electrodes ($T = 4.2$ K, $P = 3$ atm, distance $d = 1$ mm between the electrodes). b—Drift current-voltage characteristics for a pressure of 24 atm and various temperatures, for a high-frequency voltage with an amplitude of 1000 V and for $d = 1$ mm.

branches, corresponds to the case in which the space charge in the drift volume screens out the drift field nearly completely near the ion source. In this case we can again use Eqs. (1) and (2), replacing V in them by the drift voltage V_{dr} . For $V_{dr} = 25$ V, for example, we find the estimate $\bar{n} = 2 \cdot 10^9$ ions/cm³. In other words, we find a density an order of magnitude higher than in the absence of the high-frequency field. By raising the amplitude of this high-frequency field, we separate pairs with progressively smaller distances between charges, but at the same time a progressively larger number of ions manage to reach the surface of the source over half the period of this field. These ions then participate no further in the current transport. It was found experimentally that the increase in the size of the quadratic region with increasing amplitude of the high-frequency field comes to a halt when the amplitude of the vibrational motion of the ions reaches a level on the order of the thickness Δ of the ionized layer. At $T = 4$ K and at a low pressure, this condition is reached earlier for the positive ions, with the higher mobility. As the pressure is raised, the mobilities of the ions of the different signs become comparable, and the current-voltage characteristics more nearly symmetric.

The ion density in the ionized layer itself is determined by the lifetime (with respect to recombination) of electron-ion pairs. It should increase when an alternating electric field is applied (with the same stipulations regarding the loss of ions at the surface of the source). Near or beyond the end of the quadratic region of the characteristic, the average ion density in the ionized layer is on the same order of magnitude as the average density in the drift volume (the condition of a "strong" source is violated). Since the thickness of the ionized layer is smaller by a factor of about 100 than the distance between electrodes, the number of ions in the layer under these conditions is small in comparison with the number of ions in the drift volume.

4. MEASUREMENTS OF THE OPTICAL ABSORPTION

In all our optical experiments, an alternating voltage with a frequency of 200 kHz and an amplitude of 1000 V was applied to the electrodes of the test chamber. The drift voltage was 25 V, so the working point remained near the end of the quadratic region on the current-voltage characteristic at all pressures and all temperatures. The polarity of the drift voltage was reversed every 18 ms to introduce a modulation of the electron density. In the steady state, the drift gap was filled by either positive ions or electrons, depending on the sign of the drift voltage. The average charge density is given by (2). The electron densities in the ionized layer are approximately the same for the two polarities of the drift voltage, since the currents are approximately the same in these cases. The total number of electrons in the ionized layer, on the other hand, is small in comparison with the number of electrons in the drift volume, as we have already mentioned. The rise time of the current under our conditions is 15 ms, so the index of the modulation of the number of electrons in the apparatus was apparently on the order of unity.

The lasers in these experiments were used in *cw* operation. The stability of the light flux under these conditions is determined primarily by the stability of the laser current. The plot of the output power versus the laser current usually has some local extrema associated with a change in lasing mode upon a change in current and thus in the working tem-

perature of the laser crystal. The working point was chosen at one of these local maxima. The characteristic instability of the light flux, $\Delta\Phi/\Phi$, under these conditions, was on the order of 10^{-7} in a band 10^{-2} Hz wide at the working frequency. For the lasers used, the spectral linewidth of the laser output (the output linewidth) was on the order of $10-20$ cm⁻¹. This is far smaller than the width of the absorption line of interest here.

The photoresistance was operated in a constant-voltage regime. The photocurrent was converted by a preamplifier into a voltage, whose alternating part was fed to a synchronous detector. The drift voltage was used as a reference signal. The output signal from the synchronous detector was recorded as a function of the pressure in the test chamber. In these experiments, the pressure was varied linearly in time at a rate of 0.5 atm/min. Some illustrative experimental curves are shown in Ref. 14.

Several curves were recorded at a fixed temperature for each laser; the results were averaged and normalized to the constant component of the photocurrent (the dark current, i.e., the current through the photoresistance with the laser turned off, was negligible under our conditions). Figure 4 shows the results obtained in this manner for a temperature of 4.2 K. Each of the eight series of points corresponds to a given laser with a fixed output frequency. Eight series of points were also recorded at each of the temperatures 3.0 K and 2.2 K. We see from Fig. 4 that with increasing frequency of the light the absorption maximum shifts significantly toward progressively higher pressures. This behavior was found in the other two series also.

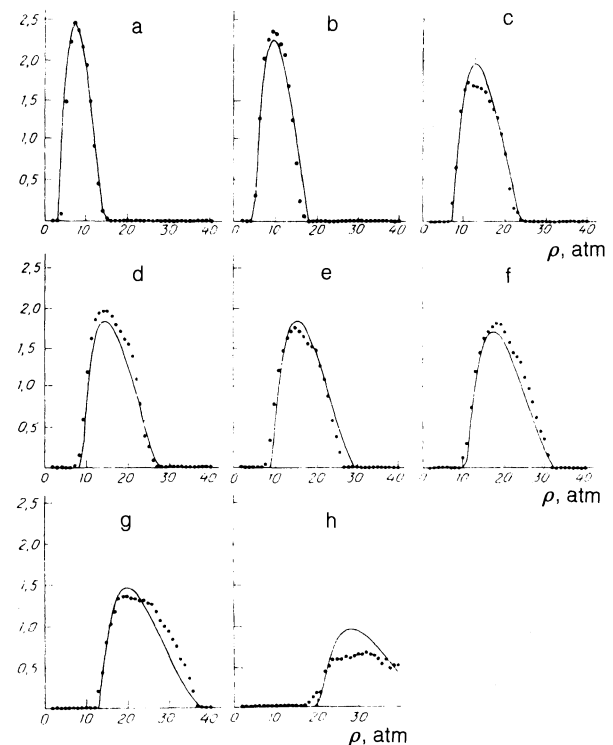


FIG. 4. Pressure dependence of the relative absorption signal (in units of 10^{-6}), averaged over several recordings, at a temperature of 4.2 K and at various wavelengths: a—8.5 μm ; b—7.8 μm ; c—7.03 μm ; d—6.7 μm ; e—6.54 μm ; f—6.3 μm ; g—5.97 μm ; h—5.3 μm . The solid lines here are the best approximation in the model discussed in the text.

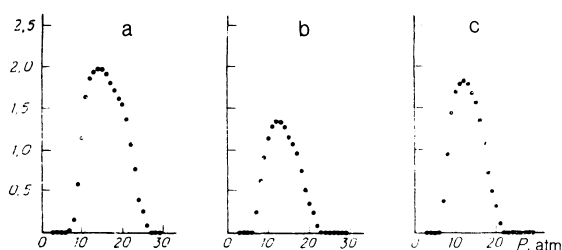


FIG. 5. Relative absorption signal versus the pressure for a laser wavelength of $6.7 \mu\text{m}$ and various temperatures: a—4.2 K; b—3.0 K; c—2.2 K.

Figure 5 shows the temperature dependence of the absorption. Shown here are experimental data for various temperatures at a fixed light frequency, i.e., for a given laser. In comparing the curves in Fig. 5, we should bear in mind that the conductance of the photoresistance decreases with decreasing temperature, so it is necessary to increase the voltage across the photoresistance in order to obtain signals large enough in comparison with the noise. These changes lead to changes in the differential sensitivity of the photoresistance, and these changes are the primary reason for the differences between the maximum values of the normalized absorption signals at the various temperatures.

Working from the data in Fig. 4 (and the corresponding data for other temperatures), we can get an idea of the behavior of the absorption as function of the frequency of the incident light at constant values of the pressure and the temperature. In other words, we can get an idea of the shape of the absorption line in its usual understanding. The number of points on curves of this type is determined by the number of lasers. Also shown in Fig. 6 are data for a pressure of 12 atm at various temperatures; shown in Fig. 7 is a series of curves for a fixed temperature and different pressures.

The absorption line is roughly symmetric. It has a

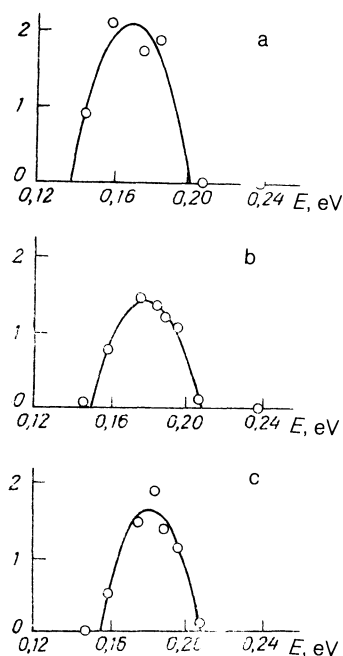


FIG. 6. Absorption spectra at a pressure of 12 atm and various temperatures: a—4.2 K; b—3.0 K; c—2.2 K.

broad, gently sloping top, with no significant wings. We accordingly approximated the shape of this line by means of parabolic arcs (the solid lines in Fig. 6 and 7). This approximation conveys the shape of the maximum and the width of the line at half-maximum fairly well. There is no point in introducing additional parameters for the line wings, which we do not observe.

As the temperature is lowered, the absorption line shifts toward a higher energy (Fig. 6). The width of the line at half-maximum, on the other hand, decreases slightly, from about 0.048 eV at 4.2 K to 0.040 eV at 2.2 K, at an average transition energy of about 0.18 eV (at such large widths, it might be more appropriate to speak in terms of an absorption band instead of a line). We see from Fig. 7 that as the pressure is raised at a fixed temperature the line undergoes a systematic shift up the energy scale, as it should if the equilibrium radius of the bubble decreases with the pressure. We also note that the area under the absorption line decreases with increasing pressure. We believe that this effect stems from a decrease in the index of the modulation of the electron density. As we mentioned earlier, the oscillator strength

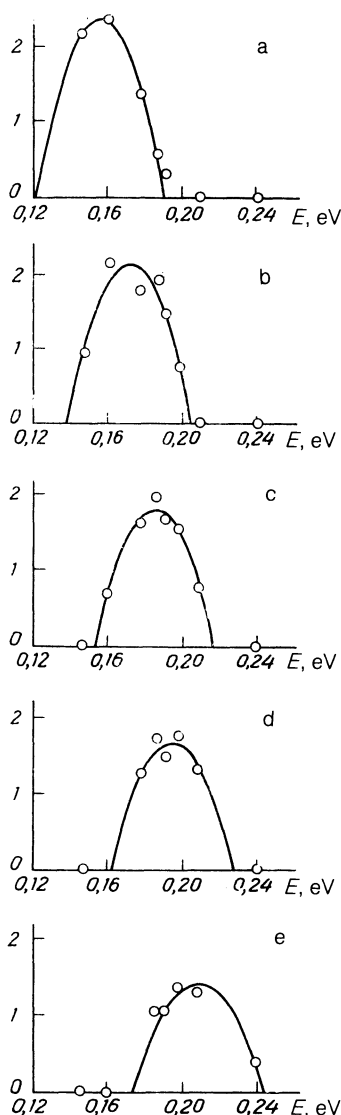


FIG. 7. Absorption spectra at 4.2 K and various pressures; a—9 atm; b—12 atm; c—15 atm; d—18 atm; e—22 atm.

for an electron in a bubble remains essentially constant as the bubble radius decreases with pressure in our range of parameter values, according to Ref. 10.

The strong alternating electric field in which these measurements were carried out could in principle have altered the observed characteristics of the absorption line. To test this possibility, we recorded an absorption signal as a function of the pressure at amplitudes of 1000 V/cm (the standard amplitude in all our experiments) and 500 V/cm as a function of the pressure. Here we used the laser with the output wavelength of 6.7 μm (among the lasers which we used, this one had the highest power and the best stability). At the lower field amplitude, the decrease in the electron density caused the absorption signal to decrease by a factor of nearly two, but there were no changes in the width or shape of the curve.

5. ANALYSIS AND DISCUSSION OF THE RESULTS

Because of the unavoidable gaps in our data (as a result of the limited set of lasers and the absence of an exact calibration of the absolute absorption level), and in face of the extremely large relative width of the line which we studied, we cannot unambiguously determine the dependence of the position and width of the line as a function of the pressure over the entire pressure range studied (2–40 atm). On the other hand, we can determine how well our results agree with theoretical predictions regarding electron bubbles. For this comparison, we can use all the data which we have.

To make this comparison, we go back to the bubble model which has been studied in most detail: a bubble with sharp boundaries, with an equilibrium radius a determined by the condition for a minimum total energy, written in the form

$$E_{1s} + \frac{4}{3}\pi a^3 P + 4\pi a^2 \sigma, \quad (4)$$

Here E_{1s} is the energy of the ground state of the electron in the spherical potential well of radius a , with a square potential of depth U_0 (equations relating E_{1s} and E_{1p} to the parameters a and U_0 can be found in Schiff,²¹ among other places). The second term here is the work which must be performed in opposition to the pressure P in the liquid in order to form the bubble. The third term incorporates the surface energy of the bubble. The correction to the energy for the polarization of the liquid is being ignored here, since it is small.

The most important parameter of the model is the surface tension of the bubble, σ . Not only the equilibrium radius of the bubble but also the frequency of its natural vibrations depends on this parameter. According to Refs. 10 and 11, the width and shape of the absorption line corresponding to the $1s \rightarrow 1p$ electron transition therefore also depend on this parameter. This is true even at nonzero temperatures. Thermal vibrations of the bubble, on the other hand, cause σ to vary with the temperature. Estimates in the spirit of the theory of Atkins²² show that these changes are by no means small in the temperature region of importance here, 2–4 K. One might suggest that in this temperature region the condition $\omega\tau \ll 1$ holds, where τ is the time scale of the relaxation to thermal equilibrium at the scale of the bubble, for the lowest-frequency vibrations of the bubble, in particular, for the breathing and quadrupole modes, with natural frequencies

$\omega \approx 10^{10} \text{ s}^{-1}$. In this case both the equilibrium radius and the frequencies of the breathing and quadrupole modes are determined by the value of σ at the given temperature. These two modes play a special role because these are the modes, according to Refs. 10 and 11, which determine the widths and positions of the lines corresponding to the $1s \rightarrow Np$ transitions (while the values of σ are determined primarily by the higher-frequency vibrational modes with a vastly greater statistical weight). For these reasons we attribute the thermal shift of the absorption line to a change in the equilibrium radius of the bubble, found from (3), where σ is some function of the temperature (and, of course, the pressure).

The parameter U_0 also changes upon a variation in the pressure and the temperature. In the simplest model (the so-called optical approximation) the quantity U_0 is proportional to the helium density. The experiments of Ref. 23 yield a ratio $U_0 = 1.02 \text{ eV}$ for a density of 0.145 g/cm^3 .

We can thus use Eq. (3) along with the functions $U_0(P)$ and $\sigma(P)$ to determine the pressure dependence of the equilibrium bubble radius.

There has been no detailed theoretical study of the shape of the absorption line. Fowler and Dexter⁷ assumed a Gaussian shape and estimated a half-width of 0.01 eV for it (at a temperature of 1.25 K). The linewidth has been studied in most detail by Fomin¹⁰ (on the basis of a model bubble with sharp boundaries). A linewidth set by vibrations of the bubble (zero-point and thermal) was calculated by perturbation theory. The leading role is played by the breathing and quadrupole modes, since among all the spherical harmonics only these modes make a nonzero correction to the energy of the electron transition from the s state to the p state in the approximation linear in the amplitude of the corresponding harmonic, ξ_i . Average values of ξ_i at high temperatures (high in comparison with the frequencies ω_i) were found from $\overline{\xi_i^2} = T/K_i$, where K_i is the stiffness of the corresponding vibrational mode. The stiffnesses were determined in the harmonic approximation. Only the corrections to E_{1s} and E_{1p} which were linear in ξ_i were considered in the calculations of the second moment M_2 (a measure of the dispersion) of the line. The absorption line is symmetric in this approximation and does not have a Gaussian shape. It is centered on the energy of the transition in a bubble of equilibrium radius. Expressions for K_i , M_2 , and ω_i are given in the Appendix.

We calculated the pressure dependence of the transition energy in a bubble of equilibrium radius using expression (3) and setting $U_0(p) = \text{const} = 1.135 \text{ eV}$. This value corresponds to a helium density 0.161 g/cm^3 . We also set $\sigma(P) = \text{const}$ with several values of σ . We calculated M_2 from Fomin's theory for the same values of U_0 and σ . The results are shown in Fig. 8 in comparison with the parameter values found for the series of curves in Fig. 7. We see that by choosing the function $\sigma(P)$ appropriately one can achieve a fairly good description of the position of the line, while the theoretical values of the measure of dispersion are well below the experimental values (such a comparison for temperatures of 3 and 2.2 K would lead to an even greater discrepancy, since, as we have already mentioned, the linewidth found experimentally increases more slowly than $T^{1/2}$ with the temperature).

Let us assume that there exists an additional mecha-

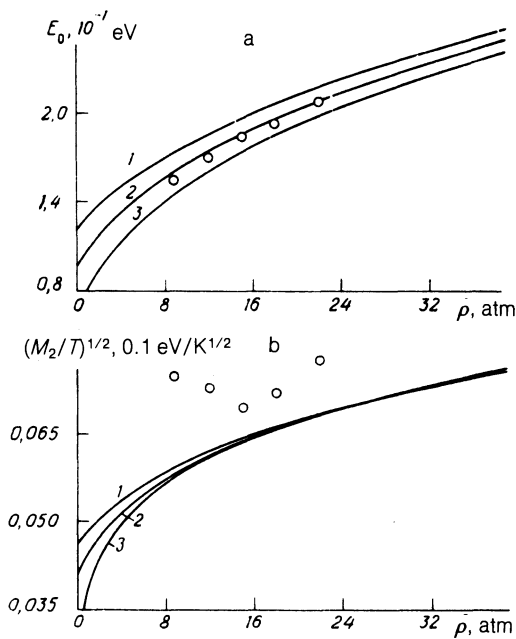


FIG. 8. a: Position of the center of the absorption line versus the pressure as calculated in a model with $U_0 = \text{const} = 1.135 \text{ eV}$ and $\sigma = \text{const}$. b: The quantity $(M_2/T)^{1/2}$ as calculated in the approximation of Ref. 10 for the same values of U_0 and σ . 1–3— $\sigma = 0.5, 0.3,$ and 0.1 erg/cm^2 , respectively. The points are experimental values found from Fig. 7.

nism for line broadening. While causing a broadening of the absorption line in a symmetric fashion, it does not change the position of the center of the line. Working under this assumption, we can attempt to describe all the data which we have obtained, after first making some simple assumptions regarding the pressure dependence of the parameters of the model.

Let us assume that U_0 is proportional to the density of the helium, as in the optical model. In order to introduce an dependence $\sigma(P)$, we assume that σ depends on the helium density in a linear way, $\sigma(P) = \sigma_0 + \sigma_1 \rho(P)$, at a fixed temperature. Consequently, the parameters σ_0 and σ_1 determine the position of the center of the line as a function of the pressure, $E_0(P)$, at a fixed temperature. We are taking data on the density of helium from Ref. 24.

We further assume that the linewidth at W half-maximum is some linear function of the pressure, and we describe the shape of the absorption line, as above (Figs. 6 and 7), by a parabolic arc defined by

$$f(x, W) = \begin{cases} (3/4x_m^3)(x_m^2 - x^2), & |x| < x_m \\ 0, & |x| > x_m \end{cases} \quad (5)$$

where $x_m = W/2^{1/2}$. The area under this curve is equal to one, and the corresponding measure of dispersion is $M_2 = W^2/10$.

It should of course be kept in mind that the index of the electron density modulation in our experiments generally depends on the pressure at a fixed temperature. As a result, the area under the absorption curve varies with pressure (Fig. 7). Unfortunately, we were unable to measure this quantity by an independent method. Since this quantity does not vary greatly (by only a factor of 1.5–2) over the pressure range of interest here, we assumed in describing the experimental data that the modulation index is a linear function of

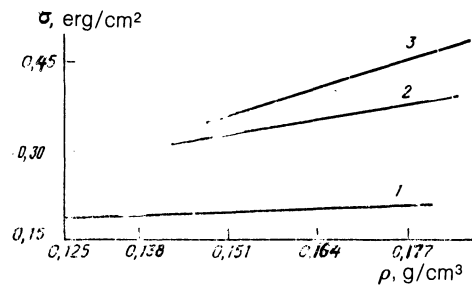


FIG. 9. Calculated values of σ as a function of the helium density at three temperatures: 1—4.2 K; 2—3.0 K; 3—2.2 K.

the pressure. In this manner we obtain two more adjustment parameters. Our model thus has a total of six adjustment parameters. The success of this model in describing the experimental data is illustrated in Fig. 4 for a temperature of 4.2 K.

Figure 9 shows curves of the effective surface tension of the bubble boundary, σ , versus the helium density for three values of the temperature, according to our model. Figure 10 shows results on the pressure dependence of the position of the center of the line at the same temperatures. We see that these results agree well with the experimental data of Grimes and Adams on the photomobility at a temperature of 1.25 K. Those data are also shown in this figure. Figure 11 compares the values of the measure of dispersion of the absorption line, found from our data as $M_2 = W^2/10$, and theoretical values of the measure of dispersion calculated in Fomin's approximation for the same values of σ and U_0 .

We thus see that if we assume the absorption line to be symmetric then our data on the position of the line can be described by a very simple bubble model with sharp boundaries. The curves of the surface tension of the bubble versus the density of the liquid which arise in this description have a plausible shape (Fig. 9). However, these curves cannot be regarded as completely reliable until we find a clear picture of the linewidth. Our assumption that the additional line-broadening mechanism (other than that discussed in Ref. 10) does not shift the center of the line may be wrong. A possible asymmetry of the line in the case of a large linewidth creates some uncertainty regarding the extent to which the center of the line (the first moment) is shifted with respect to the transition energy in a bubble of equilibrium radius. Cor-

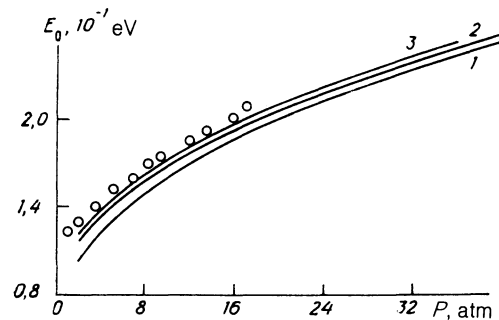


FIG. 10. Position of the center of the absorption line as a function of the pressure according to calculations from our experimental data with the help of the model described in the text, for three temperatures. The curve labels have the same meaning as in Fig. 9. The points are data taken from Fig. 2a of Ref. 13 ($T = 1.25 \text{ K}$).

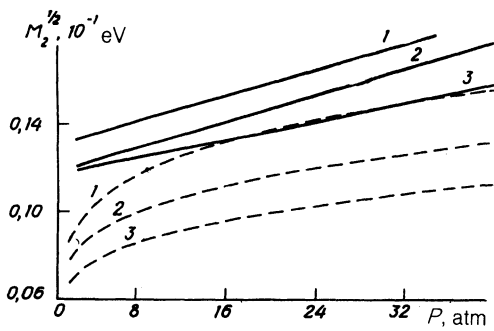


FIG. 11. Theoretical values of $M_2^{1/2}$ versus the pressure. Solid lines—Calculated from our experimental data; dashed lines—calculated in the approximation of Ref. 10 for the same values of U_0 and σ . The curve labels have the same meaning as in Fig. 9.

respondingly, we find an uncertainty in the value of σ . This uncertainty is comparable to the range of values which we found for this quantity.

Figure 12 compares the widths of the absorption lines at the temperatures which we studied, at a pressure of 12 atm, with the linewidth at the same pressure but a lower temperature, according to an estimate from Fig. 1 of Ref. 13. Also shown here are results calculated in Fomin's approximation [the corresponding equations are given in the Appendix; we used the values of σ which we found in the calculations (Fig. 9)]. An extrapolation of our data to $T = 1.25$ K leads to a value only negligibly different from the value found by Grimes and Adams. This difference probably does not go beyond the experimental errors. It is nevertheless clear that Fomin's theory¹⁰ systematically underestimates the linewidths, by an average factor of two in comparison with the experimental values.

Working in a theory based on an obviously simplified model, we of course cannot hope to find an exact description of all the experimental spectral characteristics. However, it does seem to us that the discrepancy described above could be reduced substantially or perhaps eliminated completely, even on the basis of a model bubble with sharp boundaries. The reasoning here is that the theory of Ref. 10 takes into account the contribution to the dispersion of the absorption line in a first-order perturbation theory in the amplitudes of the spherical harmonics. This contribution is zero except for the breathing and quadrupole modes. The second-order contribution from, say, the breathing mode is small in comparison with the first-order contribution by a ratio $(\xi_0/a)^2$ (in

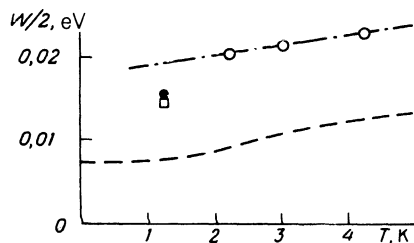


FIG. 12. Half-width of the absorption line at a pressure of 12 atm and at various temperatures. O—Data of the present study; ●—data of Ref. 13; □— $M_2^{1/2}$ at the same pressure, from Ref. 13; dashed line— $M_2^{1/2}$ according to a calculation in the approximation of Ref. 10 for the same conditions.

order of magnitude). It is of the order of $(\hbar\omega_0)^2$ at $T \ll \hbar\omega_0$ and of the order of T^2 at higher temperatures. In second order, however, all the vibrational modes make a nonzero contribution to the dispersion. There are several hundred such modes, so their resultant contribution may prove comparable to the first-order contribution. Zero-point vibrations will increase in importance here because of the increase in the average frequency of the oscillators which contribute substantially to the linewidth. As a result, the temperature dependence of the linewidth at liquid-helium temperatures will be weaker than $T^{1/2}$, in agreement with experiment.

The symmetry of the ground state of an electron bubble is a matter of fundamental importance. In the absence of spherical symmetry, bubbles in a strong electric field would become oriented. This orientation might lead to a dependence of the absorption spectrum on the orientation of the polarization plane of the light with respect to the electric field. The beams from the lasers of the type which we used are usually polarized in such a way that the electric vector in the light wave lies in the plane of the p - n junction of the laser. In some special experiments, we monitored the polarization of the beam from a laser with a wavelength $7.03 \mu\text{m}$. We carried out measurements in two layouts of the apparatus. In the first layout (which was the standard layout for all our experiments), the plane of the p - n junction of the laser was perpendicular to the electric field in the test chamber. In the second layout, it was parallel to this field. At an optical-fiber length 60 mm, about 0.8 of the intensity of the transmitted light should retain the original polarization, according to estimates of the people who fabricated the fiber. The recordings of the absorption signal as a function of the pressure made in the two layouts were found to be the same, within the experimental error.

We wish to thank L. N. Butvin for fabricating the AgCl fiber and V. F. Kocherov and N. B. Zaletaev for furnishing the photodetector. We are particularly indebted to I. I. Zsavitkii for furnishing the semiconductor lasers and to I. A. Fomin for useful discussions.

APPENDIX

The following expression was derived for the measure of dispersion of the $1s$ - $1p$ absorption line in Ref. 10:

$$M_2 = \overline{(E - E_{1s}^{1p})^2} = U_0 a^2 a^4 [(R_{1s}^2 - R_{1p}^2)^2 \xi_0^2 + 4 R_{1p}^4 \xi_0^2]. \quad (6)$$

Here R_{1s} and R_{1p} are values of the radial parts of the electron wave functions at $r = a$ in the $1s$ and $1p$ states, respectively. Using the explicit expressions for these functions, along with equations for the energy eigenvalues E_{1s} and E_{1p} (Ref. 21), we can write these quantities in the form in which they were actually used in the calculations of this paper:

$$U_0 a^2 R_{1s}^2 = \frac{\hbar^2}{ma^3} \frac{q_{1s} k_{1s}^2}{1 + q_{1s}}, \quad (7)$$

$$U_0 a^2 R_{1p}^2 = \frac{\hbar^2}{ma^3} \frac{k_{1p}^2 (1 + q_{1p})^2}{3 + 3q_{1p} + q_{1p}^2} \quad (8)$$

[$(q_{1s}^2 = -2ma^2 \hbar^{-2} E_{1s}, k_{1s}^2 = 2ma^2 \hbar^{-2} (U_0 + E_{1s}),$ and there are corresponding expressions for q_{1p} and k_{1p}].

The eigenfrequencies ω_0 and ω_2 were calculated completely in Ref. 10 only for the $P = 0$ case. Corresponding calculations for arbitrary pressures lead to the expressions

$$\omega_0^2 = \frac{1}{\rho a^2} \left[\left(P + \frac{2\sigma}{a} \right) \left(\frac{1+4q}{1+q} - \frac{k^2}{q(1+q)^2} \right) + P \right], \quad (9)$$

$$\omega_2^2 = \frac{6}{\rho a^2} \left[\left(P + \frac{2\sigma}{a} \right) \left(\frac{k^2(3+3q+q^2)}{3(1+q)^2} - \frac{1}{1+q} \right) - P \right] \quad (10)$$

(here $q = q_{1s}$, $k = k_{1s}$). The "stiffnesses" of these modes are calculated as $K_i = \mu_i \omega_i^2$, where the effective masses μ_i are, respectively,

$$\mu_0 = 4\pi\rho a^3, \quad \mu_2 = \frac{4}{15}\pi\rho a^3.$$

¹R. A. Ferrel, Phys. Rev. **108**, 167 (1957).

²V. B. Shikin, Usp. Fiz. Nauk **121**, 457 (1977) [Sov. Phys. Usp. **20**, 226 (1977)].

³J. Jortner, N. R. Kestner, S. A. Rice, and M. H. Cohen, J. Chem. Phys. **43**, 2614 (1965); Hiroike Kazuo, N. R. Kestner, S. A. Rice, and J. Jortner, J. Chem. Phys. **43**, 2625 (1965).

⁴B. F. Springell, M. H. Cohen, and J. Jortner, Phys. Rev. **159**, 183 (1967).

⁵R. C. Clark, Phys. Lett. **16**, 42 (1965).

⁶L. D. Landau and E. M. Lifshitz, *Quantum Mechanics: Non-Relativistic Theory*, Nauka, Moscow, 1989 (previous editions of this book have been published in English translation by Pergamon, New York).

⁷W. B. Fowler and D. L. Dexter, Phys. Rev. **176**, 337 (1968).

⁸T. Miyakawa and D. L. Dexter, Phys. Rev. A **1**, 513 (1970).

⁹I. A. Fomin, Pis'ma Zh. Eksp. Teor. Fiz. **6**, 715 (1967) [Sov. Phys. JETP **6**, 196 (1967)].

¹⁰I. A. Fomin, *Study of Optical and Acoustic Phenomena in Quantum Liquids. Dissertation*, ITF Akad. Nauk SSSR, Moscow, 1968.

¹¹B. Du Vall and V. Celli, Phys. Rev. **180**, 276 (1969).

¹²J. A. Northby and T. M. Sanders, Jr., Phys. Rev. Lett. **18**, 1184 (1967).

¹³C. C. Grimes and G. Adams, Phys. Rev. B **41**, 6366 (1990).

¹⁴A. Ya. Parshin and S. V. Pereverzev, Pis'ma Zh. Eksp. Teor. Fiz. **52**, 905 (1990) [JETP Lett. **52**, 282 (1990)].

¹⁵I. I. Zasavitskiĭ, Zarubezh. Radioelektron. **10**, 74 (1974).

¹⁶V. K. Tkachenko and A. I. Filimonov, Prib. Tekh. Eksp. No. 5, 203 (1961).

¹⁷R. G. Arkhipov and A. I. Shal'nikov, Zh. Eksp. Teor. Fiz. **37**, 1247 (1959) [Sov. Phys. JETP **10**, 888 (1960)].

¹⁸A. I. Shal'nikov, Zh. Eksp. Teor. Fiz. **47**, 1727 (1964) [Sov. Phys. JETP **20**, 1161 (1965)].

¹⁹G. Careri and F. Gaeta, Nuovo Cim. **20**, 152 (1961).

²⁰D. G. Onn and M. Silver, Phys. Rev. **181**, 295 (1969).

²¹L. F. Schiff, *Quantum Mechanics*, McGraw-Hill, New York, 1968.

²²K. R. Atkins, Can. J. Phys. **31**, 1165 (1953).

²³M. A. Woolf and G. W. Rayfield, Phys. Rev. Lett. **15**, 235 (1965).

²⁴B. N. Esel'son, V. N. Grigor'ev, V. G. Ivantsov, and E. Ya. Rudavskii, *Properties of Liquid and Solid Helium*, [in Russian] Naukova Dumka, Kiev, 1982.

Translated by D. Parsons